## Chern numbers and chiral anomalies in Weyl butterflies

Sthitadhi Roy, Michael Kolodrubetz, Joel E. Moore, and Adolfo G. Grushin

The Hofstadter butterfly of lattice electrons in a strong magnetic field is a cornerstone of condensed matter physics, exploring the competition between periodicities imposed by the lattice and the field. In this work we introduce and characterize the Weyl butterfly, which emerges when a large magnetic field is applied to a three-dimensional Weyl semimetal. Using an experimentally motivated lattice model for cold atomic systems, we solve this problem numerically. We find that Weyl nodes reemerge at commensurate fluxes and propose using wavepackets dynamics to reveal their chirality and location. Moreover, we show that the chiral anomaly – a hallmark of the topological Weyl semimetal – does not remain proportional to magnetic field at large fields, but rather inherits a fractal structure of linear regimes as a function of external field. The slope of each linear regime is determined by the difference of two Chern numbers in gaps of the Weyl butterfly and can be measured experimentally in time of flight.

Introduction – The search for novel phenomena in condensed matter is often spurred by two or more competing physical effects acting on comparable length scales. A central example is the response of fermions on a lattice to an external magnetic field. When the magnetic length  $l_B$  becomes comparable to the lattice spacing a, the energy spectrum displays a fractal structure known as the Hofstadter butterfly [1]. The Hofstadter spectrum is periodic in applied field, with period given by one magnetic flux quantum  $\Phi_0 = h/e$  per unit cell. Furthermore, the gaps that separate each magnetic subband are characterized by a two-dimensional topological Chern number.

The presence of topological invariants generally signals novel condensed matter phenomena. Topological insulators [2, 3] and more recently gapless Weyl and Dirac semimetals [4–6] are understood in terms of topological invariants. The latter metallic states host protected band touching points (nodes) that disperse linearly with momentum. Each node is identified by either left or right chirality, a quantum number that resembles the valley degree of freedom in graphene, and the numbers of nodes with left and right chirality are equal.

Although the sum of right and left handed fermions has to be conserved, non-orthogonal magnetic ( $\mathbf{B}$ ) and electric ( $\mathbf{E}$ ) fields pump one chirality to the other at a rate proportional to  $\mathbf{E} \cdot \mathbf{B}$ , so that their difference is not conserved. This phenomenon, known as the chiral anomaly [7, 8], distinguishes conventional metals from topological ones; while the former display positive longitudinal magnetoresistance as a function of magnetic field, the chiral anomaly manifests as negative magnetoresistance in the latter [9, 10]. This phenomenon is consistent with recent mangetotransport measurements [11–19] that include the TaAs class of Weyl semimetals [20–26], Na<sub>3</sub>Bi [27–30], Cd<sub>3</sub>As<sub>2</sub> [31–37] and ZrTe<sub>5</sub> [38].

The current understanding of Weyl fermions in external electromagnetic fields is well developed both in

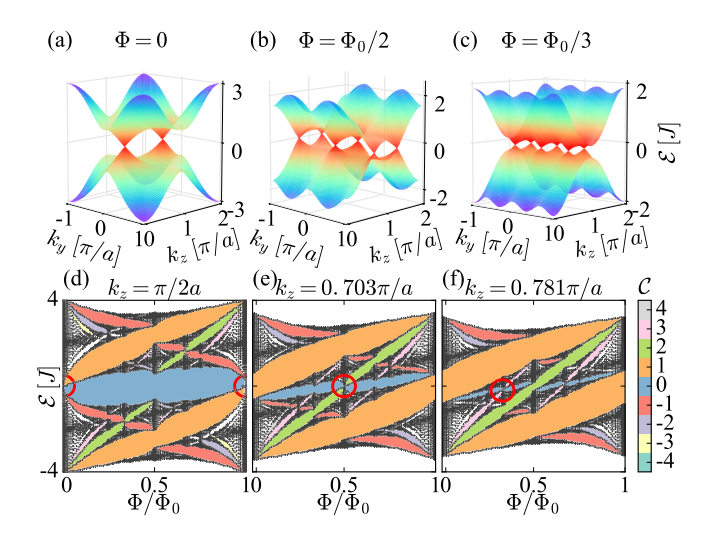


FIG. 1. Energy spectra of Weyl fermions in a magnetic field, as obtained from Eq. (2). (a)-(c) New Weyl nodes emerge at certain commensurate fluxes per plaquette with an additional q-fold degeneracy (see text). (d)-(f) Hofstadter spectrum for the  $k_z$  values where the Weyl cones appear for the corresponding fluxes shown in (a)-(c). The isolated zeroth Landau level can also be seen around the Weyl nodes highlighted by the red circles. The colors in the butterflies denote the Chern number  $\mathcal C$  in the gap.

the linear response regime [39–46] and the Landau level limit [8, 45, 47–49]. However, it is so far not known how Weyl fermions behave as the Hofstadter regime is approached and what is the fate of the chiral anomaly in this limit. For instance, the theorem preventing the non-renormalization of the chiral anomaly beyond one-loop imposing the familiar  $\mathbf{E} \cdot \mathbf{B}$  form [7], must break down once lattice effects become important, as any functional dependence of the anomaly on  $\mathbf{B}$  must be periodic in units of  $\Phi_0$  per unit cell.

In this work we fill in this gap by investigating the fate of Weyl fermions as they approach the Hofstadter regime

<sup>&</sup>lt;sup>1</sup>Max-Planck-Institut für Physik komplexer Systeme, Nöthnitzer Straße 38, 01187 Dresden, Germany <sup>2</sup>Department of Physics, University of California, Berkeley, CA 94720, USA <sup>3</sup>Materials Sciences Division, Lawrence Berkeley National Laboratory, Berkeley, CA 94720, USA

 $(l_B \sim a)$  with special focus on the chiral anomaly. We are motivated not only by fundamental interest [50–57] in the problem but also by the experimental possibility to access this regime in cold atomic systems [58]. Using a model tightly connected to the experimental proposal in Ref. [58] we track the chiral anomaly through the rate of pumped chiral charge. We find that this quantity is proportional to magnetic field only as a fractal of linear regimes with quantized slope that occur around emergent Weyl nodes at commensurate fluxes. We connect this observation to Chern numbers in the gaps of the Weyl butterfly – the spectrum obtained when applying large fluxes to the Weyl semimetal – and show how both these Chern numbers and the chiral anomaly may be directly measured with cold atoms.

Weyl semimetal in magnetic fields – To describe a Weyl semimetal, we employ a two-band Hamiltonian of spinless fermions on a cubic lattice with Hamiltonian  $\mathcal{H}_{\mathbf{k}} = \mathbf{d}_{\mathbf{k}} \cdot \boldsymbol{\sigma}$ ,

$$\mathbf{d_k} = -\{J_2 \sin k_x, J_2 \sin k_y, -M + J_1 \sum_{i=x,y,z} \cos k_i\}.$$
 (1)

This model breaks time-reversal symmetry and is motivated by that in Ref. [58], which is composed of the two time reversal partners of Eq. (1) separated in momentum space. It has a pair of linearly dispersing Weyl cones at  $\mathbf{k} = \{0, 0, \pm \cos^{-1}(M/J_1 - 2)\}$  for  $1 < |M/J_1| < 3$ , and two pairs of Weyl cones for  $|M/J_1| < 1$ . We use  $J_2 = J_1 = J$  and M/J = 2 for the remainder of this paper. Fig. 1(a) shows the band structure in the  $(k_y, k_z)$  plane. Inspection of Eq. (1) reveals that this model is constructed from Chern insulators in the  $(k_x, k_y)$  plane with a  $k_z$  dependent gap such that the Chern number  $\mathcal{C}_{k_z}$  changes whenever a Weyl node is crossed, as shown by the dashed line in Fig. 2b.

We now consider applying a magnetic field  $\mathbf{B} \parallel \hat{z}$  with flux  $\Phi = \Phi_0 p/q$  per plaquette, equivalent to an Aharonov-Bohm phase of  $\phi = 2\pi p/q$  upon tunneling around a plaquette. In the Landau gauge,  $\mathbf{A} = \Phi x \hat{y}$ , the Hamiltonian becomes

$$\mathcal{H}_{\mathcal{WH}} = \begin{pmatrix} \mathcal{M}_1 & \mathcal{R}/2 & 0 & \cdots & \mathcal{S}/2 \\ \mathcal{R}/2^{\dagger} & \mathcal{M}_2 & \mathcal{R}/2 & \cdots & 0 \\ \vdots & \ddots & \ddots & \vdots \\ \mathcal{S}^{\dagger}/2 & 0 & \cdots & \mathcal{R}^{\dagger}/2 & \mathcal{M}_q \end{pmatrix};$$

$$\mathcal{M}_n(k_y, k_z) = [M - J(\cos(k_y + \phi n) + \cos k_z)]\sigma^z - J\sin(k_y + \phi n)\sigma^y;$$

$$\mathcal{R} = -J(\sigma^z - i\sigma^x); \quad \mathcal{S}(k_x) = -J(\sigma^z + i\sigma^x)e^{-ik_x}. \quad (4)$$

Each  $k_z$  exhibits a Hofstadter-like spectrum [59], as depicted in Fig. 1. We refer to this spectrum as the Weyl butterfly.

One unexpected aspect of the Weyl butterfly is that, for certain fluxes, new pairs of Weyl nodes emerge with q-fold degeneracy. [60] In Fig. 1(d)-(f) we highlight some

of the emergent Weyl nodes that cross near  $\mathcal{E}=0$  for particular values of  $k_z$ . The emergence of such new Weyl nodes is related to the fractal structure of the butterfly, while the q-fold degeneracy comes from noting that the shift  $k_y \rightarrow k_y + 2\pi p/q$  in Eq. (2) amounts to changing **A** in steps of  $\Phi$ , which has no effect on the spectrum. Since q such translations traverse the entire BZ, there should be q copies of the spectrum. [61] Perturbing the flux around one of these emergent Weyl nodes splits it into Landau levels dispersing along  $k_z$ , including a chiral zeroth Landau level [8]. As the flux is further increased, the Landau levels split and merge with those of the upcoming Weyl node, a feature which we explore in more detail later.

Chern numbers via wavepacket dynamics – An important topological invariant that characterizes Weyl semimetals both in the presence and absence of magnetic field is the Chern number in each momentum plane. An experimentally feasible probe of this invariant tailored to cold-atomic systems is the semi-classical motion of wavepackets [62, 63], which has successfully been used in both the two-dimensional Hoftsatdter [64] and Haldane [65] models. The principle is that, under the effect of an external force, a wavepacket shows a Hall drift transverse to the direction of the force with amplitude proportional to the Chern number.

Here we explore the use of such Hall-like response in cold-atomic systems to characterize the Weyl butterfly. We will discuss two different but related experimental protocols. First, we consider preparing a wavepacket that is sharply peaked around a finite momentum  $k_z$  along the axis of Weyl node separation. Such a wavepacket could be achieved experimentally by initially decreasing the lattice depth along the z-direction to create a sharp  $k_z$  peak then taking it to the desired  $k_z$  via a ramped magnetic field [66] or optical gradient [64], lattice acceleration [67], or Bragg pulse. [68] Following Ref. [62], we consider a wavepacket initially confined within a  $L_s \times L_s$ sub-region of an  $L \times L$  lattice  $(L_s < L)$  in the (x, y) plane. At t = 0, the xy-confinement is removed to give approximately uniformly-filled bands in the  $(k_x, k_y)$  plane [69] and a constant force  $\mathbf{F} = EJ/a \ \hat{y}$  is applied [64, 66, 67], analogous to that of an electric field of magnitude E acting on charged particles. The center of mass motion of a single particle wavepacket in the  $n^{\text{th}}$ -band is then governed by the semiclassical equations of motion [70]

$$\dot{\mathbf{r}}_c = \nabla_{\mathbf{k}} \mathcal{E}_{n,\mathbf{k}} - \dot{\mathbf{k}} \times \mathbf{\Omega}_{n,\mathbf{k}}; \quad \dot{\mathbf{k}} = \mathbf{F};$$
 (3)

where  $\mathcal{E}_{n,\mathbf{k}}$  and  $\Omega_{n,\mathbf{k}}$  are respectively the energy dispersion and Berry curvature of the band. The net drift of a many-fermion wavepacket under the electric field can be obtained by integrating the equation for  $\dot{\mathbf{r}}_c$  (3) over time and summing over the responses for all the filled bands. For m uniformly filled bands, the drift is [62]

$$\mathbf{r}_c(t) - \mathbf{r}_c(0) = -\frac{Et}{2\pi} \sum_{n=1}^m \mathcal{C}_n \ \hat{x} \equiv -\frac{Et}{2\pi} \mathcal{C}_m \ \hat{x}, \quad (4)$$

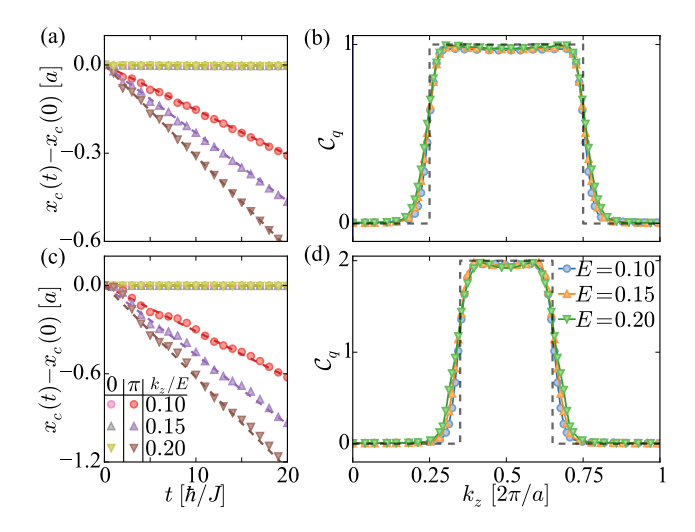


FIG. 2. Hall drift of the center of mass of a wavepacket for different values of the electric field E at two representative  $k_z$  values, 0 and  $\pi$ , along with the linear fits used to calculate  $C_q$  for q = 1 (a) and q = 2 (c). (b) and (d) show the topological transition of  $C_q$  at the positions of the Weyl nodes, as obtained from Eq. (4). For the simulations L = 128 and  $L_s = 48$ .

where  $C_n = (1/2\pi) \int dk_x dk_y \ \Omega_{n,\mathbf{k}}^z$  is the Chern number of the *n*-th band.

For flux  $\Phi$ , we can use the Hall drift of the wavepacket to measure the sum of the Chern numbers of the q lowest bands,  $\mathcal{C}_q$ , since the Weyl nodes connect the  $q^{\text{th}}$  and  $(q+1)^{\text{th}}$  bands. The Hall drift given by Eq. (4), and its corresponding  $C_q$  are shown in Fig. 2 for two different fluxes as a function of  $k_z$ . As  $k_z$  crosses a Weyl node, the  $q^{\text{th}}$  and  $(q+1)^{\text{th}}$  bands undergo a topological phase transition where the sign of the gap of the Chern insulator flips. Consequently, since there are q such Weyl points, the Chern number changes by  $\pm q$ , where the sign is determined by the chirality of the Weyl node. Thus from the wavepacket dynamics as a function of  $k_z$ , one can extract the location of the Weyl points, their chiralities, and their multiplicities.

So far we have assumed that the wavepackets are sharply-peaked as a function of  $k_z$ . In realistic experimental set-ups, it is often easier to prepare a finite-width distribution of the occupations  $W_{k_z}$ . This motivates our second protocol proposal; the control over the wave-packet spread, through an external trapping potential and/or temperature for instance, allows to infer information about the spectrum. In this case, the Hall drift with the Fermi level in the  $q^{\rm th}$  gap yields a non-quantized effective Chern number,  $\mathcal{C}_{q,\rm eff} = \sum_{k_z} \mathcal{C}_{q,k_z} W_{k_z}$ , which is the average of  $\mathcal{C}_{q,k_z}$  weighted by  $W_{k_z}$ . For instance, it is possible to create Gaussian distributions centered at  $k_z=0$  with width  $\sigma$ . For the particular case of two Weyl nodes at  $\pm K_0/2$ , we find that the dependence of the Hall drift on  $\sigma$  saturates to  $\mathcal{C}_{q,\rm eff} = \mathcal{C}_{q,k_z=\pi} - (\mathcal{C}_{q,k_z=\pi} - \mathcal{C}_{q,k_z=0})K_0/2\pi$  in the  $\sigma \to \infty$  limit and to  $\mathcal{C}_{q,\rm eff} = \mathcal{C}_{q,k_z=0}$ 

for  $\sigma \to 0$ . Varying  $\sigma$  interpolates between these limits; a simple fit can then extract the Chern number profile. A more in-depth analysis can be found in the Supplementary material.

Chiral anomalies in the Weyl butterfly acteristic property of the Weyl nodes that we dynamically characterized in the previous section is the chiral anomaly [7, 8]; non-orthogonal electric and magnetic fields pump left handed to right handed fermions at a rate  $\propto \mathbf{E} \cdot \mathbf{B} \neq 0$ . In the Landau level regime, relevant to condensed matter systems, the pumping connects two zeroth Landau levels with opposite chirality through the bottom of the band. In contrast, cold-atomic systems can naturally host a flux per plaquette that is a sizable fraction of  $\Phi_0$ , and the relevant spectrum is determined by the Weyl buttefly discussed previously. Since the spectrum satisfies  $\mathcal{E}(\Phi) = \mathcal{E}(\Phi + m\Phi_0)$  with  $m \in \mathbb{Z}$ , the linear dependence of the chiral pumping on  $\Phi$  cannot hold for all fluxes. In this section we reveal the fate of the chiral anomaly in this high-field regime which represents the main result of our work.

Our starting point is the Weyl semimetal model Eq. (1) at  $\Phi = 0$  with the chemical potential chosen to be at the Weyl nodes ( $\mathcal{E}_F = 0$ ). Upon applying a finite flux ( $\Phi/\Phi_0 \lesssim 1/4$ ) the spectrum first breaks into Landau levels (cf. Fig. 3a) that disperse as a function of  $k_z$ . Due to the chiral anomaly, if an additional electric field is applied at t = 0 satisfying  $\mathbf{E} \parallel \hat{z}$ , we expect the occupancies to shift along  $k_z$  such that left handed fermions are converted to right handed fermions via the bottom of the band. Therefore, to characterize the chiral anomaly, we find it convenient to define the chiral charge density as

$$\mathcal{N}_5 = \left(\frac{1}{L^2}\right) \sum_{k_y=0}^{2\pi} \left[ \sum_{k_z=0}^{\pi} n_{k_y, k_z} - \sum_{k_z=\pi}^{2\pi} n_{k_y, k_z} \right], \quad (5)$$

where  $n_{k_y,k_z}$  is the total number of filled fermionic states with momentum  $k_y,k_z$ . This quantity monitors the amount of charge pumped from one half of the Brillouin zone to another; its rate of increase is proportional to the applied electric field. The definition (5) implies that only the states that cross the Fermi level can contribute to the pumping of chiral charge. For  $\Phi/\Phi_0 \lesssim 1/4$  we find as expected that  $\mathcal{N}_5$  grows linearly with time (Fig. 3b). In addition, the rate of growth  $d\mathcal{N}_5/dt$  normalized by the electric field intensity is linear as a function of  $\Phi$  (Fig. 3c). So far, both of these results are consistent with the conventional chiral anomaly picture with  $d\mathcal{N}_5/dt \propto \mathbf{E} \cdot \mathbf{B}$ .

However, as the flux increased  $(\Phi/\Phi_0 > 1/4)$  we find that the linear behavior of  $d\mathcal{N}_5/Edt$  with  $\Phi$  breaks down, an observation that we now link to the properties of the emergent Weyl butterfly. As shown in Fig. 3c, several linear regimes where  $d\mathcal{N}_5/dt \propto \Phi$  appear, with unequal slopes. Each linear regime is centred around commensurate fluxes  $\Phi/\Phi_0 = p/q$ , and the slope is quantized to

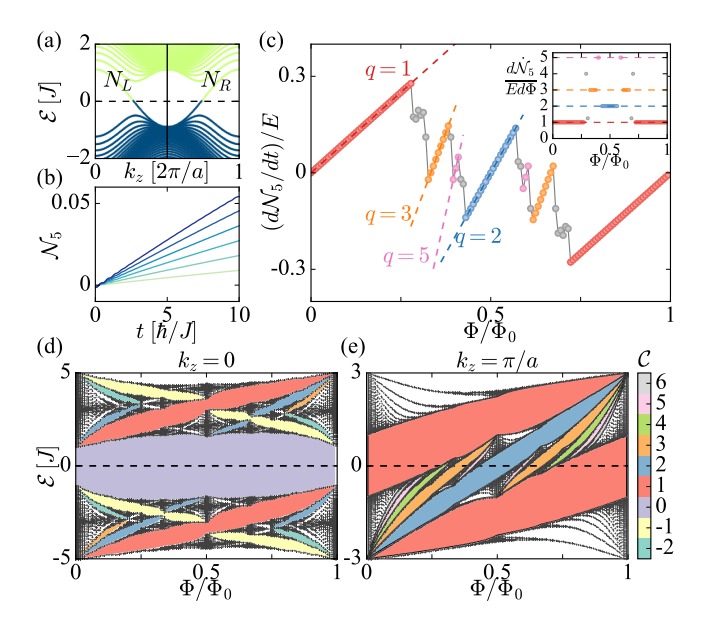


FIG. 3. Chiral anomaly of the Weyl butterfly. (a) The chiral charge counts the number difference of left and right movers  $\mathcal{N}_5 = (N_L - N_R)/L^2$ . (b)  $\mathcal{N}_5$  increases linearly with time when both E and B are applied as shown for E=0.1and fluxes  $\Phi = n\Phi_0/L$ , with n going from 1 to 6 (lighter to darker). (c) The rate of chiral charge production grows linearly with the flux with a slope q in the vicinity of certain fluxes  $\Phi$ , for which the model is a Weyl semimetal with q pairs of Weyl nodes. Linear fits are shown for the data around  $\Phi/\Phi_0 = 1, 1/2, 1/3, 2/5$  which correspond to q = 1, 2, 3, 5 respectively. The inset shows quantized plateaus corresponding to each linear rates as a function of  $\Phi$ . The simulations are performed on a cubic lattice with linear dimension L=144. (d.e) The magnitude of each plateau can be extracted from the difference between the Chern numbers in the Weyl butterfly gaps at  $k_z = 0$  and  $\pi/a$  as given by (7). The slopes in (c) are color coded to the Chern numbers colors in (d-e)

q. This is a direct consequence of the presence of q pairs of Weyl nodes, leading to q copies of the Landau levels crossing the Fermi energy. Hence, as the flux is ramped, the Landau level degeneracy grows as  $q\Phi$ , which leads to a rate of chiral charge production  $d\mathcal{N}_5/dtE \propto q\Phi$ . The full behaviour is thus composed of jumps between the linear regimes in Fig. 3 around conmensurate values of the flux for a given lattice dimension. In the thermodynamic limit the self similar fractal structure of the butterfly implies that these linear regimes should themselves form a fractal of integer valued slopes.

In order to establish a more physical understanding of the fractal nature of the anomaly we now restate our findings in a different language. Recall first that the rate of chiral charge pumping  $\dot{\mathcal{N}}_Q/E$  counts the number of chiral channels at the Fermi level. Second, we emphasize that the Weyl butterfly has, for fixed  $k_z$ , a series of gaps at  $\mathcal{E}_F=0$  (cf. Fig. 3d-e), each characterized by its Chern number  $\mathcal{C}_{k_z}$ . The Chern number determines how the density is modified when applying a magnetic field

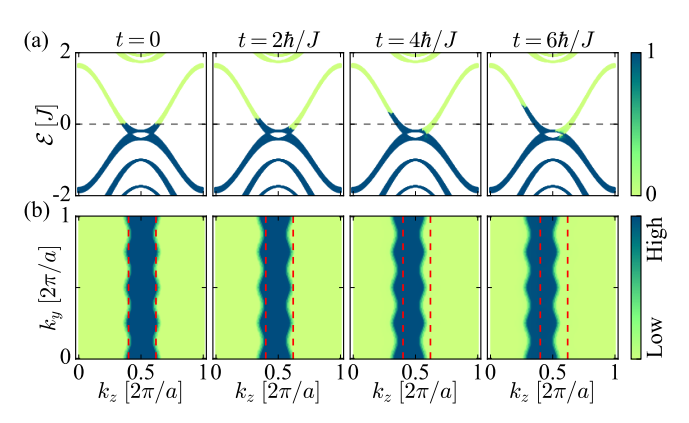


FIG. 4. (a) Evolution of occupancies in the bands after an electric field E=0.1 is turned on, showing the development of the chiral anomaly for  $\Phi=\Phi_0/4$ . The dashed horizontal line represents the Fermi level  $\mathcal{E}_F$ . (b) Time of flight occupancy profiles in the  $(k_y,k_z)$  plane in arbitrary units. The vertical dashed lines serve as a guide to the eye for the initial profile at t=0. Simulation parameters are the same as Fig. 3.

through the Streda formula [71]

$$d\rho_{\rm 2D}^{k_z}/dB_z = \mathcal{C}_{k_z}|_{\mathcal{E}_F=0}/\Phi_0 \ . \tag{6}$$

Now consider adding one flux quantum to the system  $\Delta B_z = \Phi_0/L^2$ . For  $k_z = 0$ ,  $\mathcal{C}_q = 0$ , so the density is unaffected. For  $k_z = \pi$ ,  $\mathcal{C}_q = q$ , so to increase  $\rho_{\text{2D}}$  as in Eq. (6), q conduction levels must move to the valence band. The difference must be accommodated in between these momenta, which leads to q extra chiral channels. Since, for the inversion-symmetric Weyl semimetal model defined by Eq. (1), the Weyl points always appear in  $\pm k_z$  pairs with opposite chirality, it suffices to consider  $k_z = 0$ ,  $\pi/a$ . This predicts that the chiral anomaly generalizes to

$$(1/E)d\dot{\mathcal{N}}_5/d\Phi = \mathcal{C}_{k_z=\pi/a} - \mathcal{C}_{k_z=0} , \qquad (7)$$

which is confirmed in Fig. 3c-e. Furthermore, since the butterfly at  $k_z = \pi$  consists of a fractal set of gapped Chern insulators, we see that the anomaly will become a fractal set of linear anomalies with quantized slopes in the thermodynamic limit.

We close by addressing the experimental prospects to probe the chiral anomaly. Lack of reservoirs and relaxation make transport measurements difficult, but this also helps distinguish the chiral anomaly in cold atoms from other competing effects. In practice, the most direct way to probe it is by measuring occupation numbers via time of flight experiments, which directly map out the momentum-space occupancies. [72] Fig. 4a and Fig. 4b shows the calculated band occupancies and time of flight images for  $\Phi/\Phi_0 = 1/4$  as a function of time when an electric field is applied parallel to the magnetic field at t = 0. The rate of change of  $\mathcal{N}_5$  can be monitored to

probe the chiral anomaly and experimentally access the information presented in Fig. 3.

We have shown that the chiral anomaly generalizes to a stunning quantized fractal in the highmagnetic-field limit, linking the longitudinal response characteristic of the chiral anomaly to the transverse Hall response characterized by the Chern number. The strength of each anomaly plateau is quantized to a different integer strength set by a multiple of q. Although we have used inversion symmetry in our analysis, we emphasize that this ingredient is not essential and the generalization of our results to models with several Wevl nodes is possible. In particular, since time-of-flight measurements resolve the momentum, it is in principle possible to track each pair of Weyl nodes independently to measure the chiral pumping leading to Fig. 3. Our results can be experimentally tested using existing technology in realistic models such as that in Ref. [58] or the three dimensional variant [73] of the model proposed in Ref. [74]; indeed the high magnetic field necessary for the Weyl butterfly physics lies at the heart of Ref. [58]. Finally, we expect these effects to be robust to weak experimental realities such as interactions [75, 76] and disorder [47, 77, 78] but we leave the important open question of what happens in strongly-perturbed cases for future research.

Acknowledgements – AGG acknowledges financial support from the European Commission under the Marie Curie Programme. We thank C. Kennedy for useful insights on the experimental feasibility of this proposal. MK and JEM were supported by Laboratory Directed Research and Development (LDRD) funding from Berkeley Lab, provided by the Director, Office of Science, of the U.S. Department of Energy under Contract No. DEAC02-05CH11231, and JEM acknowledges a Simons Investigator grant.

- Douglas R. Hofstadter, "Energy levels and wave functions of bloch electrons in rational and irrational magnetic fields," Phys. Rev. B 14, 2239-2249 (1976).
- [2] M. Z. Hasan and C. L. Kane, "Topological insulators," Rev. Mod. Phys. 82, 3045 (2010).
- [3] Xiao-Liang Qi and Shou-Cheng Zhang, "Topological insulators and superconductors," Rev. Mod. Phys. 83, 1057–1110 (2011).
- [4] Pavan Hosur and Xiaoliang Qi, "Recent developments in transport phenomena in Weyl semimetals," Comptes Rendus Physique 14, 857–870 (2013).
- [5] Ari M Turner and Ashvin Vishwanath, "Beyond Band Insulators: Topology of Semi-metals and Interacting Phases," arXiv:1301.0330.
- [6] Oskar Vafek and Ashvin Vishwanath, "Dirac Fermions in Solids: From High-T cCuprates and Graphene to Topological Insulators and Weyl Semimetals," Annu. Rev. Condens. Matter Phys. 5, 83–112 (2014).

- [7] Reinhold A Bertlmann, Anomalies in quantum field theory, Vol. 91 (Oxford University Press, 2000).
- [8] H.B. Nielsen and Masao Ninomiya, "The Adler-Bell-Jackiw anomaly and Weyl fermions in a crystal," Phys. Lett. B 130, 389–396 (1983).
- [9] D T Son and B Z Spivak, "Chiral anomaly and classical negative magnetoresistance of Weyl metals," Phys. Rev. B 88, 104412 (2013).
- [10] A A Burkov, "Negative longitudinal magnetoresistance in Dirac and Weyl metals," arXiv (2015), 1505.01849.
- [11] Heon-Jung Kim, Ki-Seok Kim, J.-F. Wang, M. Sasaki, N. Satoh, A. Ohnishi, M. Kitaura, M. Yang, and L. Li, "Dirac versus weyl fermions in topological insulators: Adler-bell-jackiw anomaly in transport phenomena," Phys. Rev. Lett. 111, 246603 (2013).
- [12] Xiaochun Huang, Lingxiao Zhao, Yujia Long, Peipei Wang, Dong Chen, Zhanhai Yang, Hui Liang, Mianqi Xue, Hongming Weng, Zhong Fang, Xi Dai, and Genfu Chen, "Observation of the Chiral-Anomaly-Induced Negative Magnetoresistance in 3D Weyl Semimetal TaAs," Phys. Rev. X 5, 031023 (2015).
- [13] C. Zhang, S.-Y. Xu, I. Belopolski, Z. Yuan, Z. Lin, B. Tong, N. Alidoust, C.-C. Lee, S.-M. Huang, H. Lin, M. Neupane, D. S. Sanchez, H. Zheng, G. Bian, J. Wang, C. Zhang, T. Neupert, M. Zahid Hasan, and S. Jia, arXiv:1503.02630.
- [14] Jun Xiong, Satya K. Kushwaha, Tian Liang, Jason W. Krizan, Max Hirschberger, Wudi Wang, R. J. Cava, and N. P. Ong, "Evidence for the chiral anomaly in the Dirac semimetal Na3Bi," Science 350, 413–416 (2015).
- [15] X. Yang, Y. Li, Z. Wang, Y. Zhen, and Z.-A. Xu, arXiv:1506.02283.
- [16] C. Shekhar, F. Arnold, S.-C. Wu, Y. Sun, M. Schmidt, N. Kumar, A. G. Grushin, J. H. Bardarson, R. Donizeth dos Reis, M. Naumann, M. Baenitz, H. Borrmann, M. Nicklas, E. Hassinger, C. Felser, and B. Yan, arXiv:1506.06577.
- [17] Jianhua Du, Hangdong Wang, Qianhui Mao, Rajwali Khan, Binjie Xu, Yuxing Zhou, Yannan Zhang, Jinhu Yang, Bin Chen, Chunmu Feng, and Fang Minghu, "Unsaturated both large positive and negative magnetoresistance in weyl semimetal tap," arXiv:1507.05246.
- [18] Chenglong Zhang, Cheng Guo, Hong Lu, Xiao Zhang, Zhujun Yuan, Ziquan Lin, Junfeng Wang, and Shuang Jia, "Large magnetoresistance over an extended temperature regime in monophosphides of tantalum and niobium," Phys. Rev. B 92, 041203 (2015).
- [19] H. Li, H. He, H.-Z. Lu, H. Zhang, H. Liu, R. Ma, Z. Fan, S.-Q. Shen, and J. Wang, "Negative Magnetoresistance in Dirac Semimetal Cd3As2," Nat. Commun. 7, 10301 (2016).
- [20] Hongming Weng, Chen Fang, Zhong Fang, B. Andrei Bernevig, and Xi Dai, "Weyl semimetal phase in noncentrosymmetric transition-metal monophosphides," Phys. Rev. X 5, 011029 (2015).
- [21] Shin-Ming Huang, Su-Yang Xu, Ilya Belopolski, Chi-Cheng Lee, Guoqing Chang, BaoKai Wang, Nasser Alidoust, Guang Bian, Madhab Neupane, Chenglong Zhang, Shuang Jia, Arun Bansil, Hsin Lin, and M. Zahid Hasan, "A Weyl Fermion semimetal with surface Fermi arcs in the transition metal monopnictide TaAs class," Nat. Commun. 6 (2015).
- [22] Su-Yang Xu, Ilya Belopolski, Nasser Alidoust, Madhab Neupane, Guang Bian, Chenglong Zhang, Raman

- Sankar, Guoqing Chang, Zhujun Yuan, Chi-Cheng Lee, Shin-Ming Huang, Hao Zheng, Jie Ma, Daniel S. Sanchez, BaoKai Wang, Arun Bansil, Fangcheng Chou, Pavel P. Shibayev, Hsin Lin, Shuang Jia, and M. Zahid Hasan, "Discovery of a weyl fermion semimetal and topological fermi arcs," Science **349**, 613–617 (2015).
- [23] B. Q. Lv, H. M. Weng, B. B. Fu, X. P. Wang, H. Miao, J. Ma, P. Richard, X. C. Huang, L. X. Zhao, G. F. Chen, Z. Fang, X. Dai, T. Qian, and H. Ding, "Experimental Discovery of Weyl Semimetal TaAs," Phys. Rev. X 5, 031013 (2015).
- [24] Su-Yang Xu, Nasser Alidoust, Ilya Belopolski, Zhu-jun Yuan, Guang Bian, Tay-Rong Chang, Hao Zheng, Vladimir N. Strocov, Daniel S. Sanchez, Guoqing Chang, Chenglong Zhang, Daixiang Mou, Yun Wu, Lunan Huang, Chi-Cheng Lee, Shin-Ming Huang, BaoKai Wang, Arun Bansil, Horng-Tay Jeng, Titus Neupert, Adam Kaminski, Hsin Lin, Shuang Jia, and M. Zahid Hasan, "Discovery of a weyl fermion state with fermi arcs in niobium arsenide," Nat. Phys. 11, 748-754 (2015).
- [25] B. Q. Lv, N. Xu, H. M. Weng, J. Z. Ma, P. Richard, X. C. Huang, L. X. Zhao, G. F. Chen, C. E. Matt, F. Bisti, V. N. Strocov, J. Mesot, Z. Fang, X. Dai, T. Qian, M. Shi, and H. Ding, "Observation of Weyl nodes in TaAs," Nat. Phys. 11, 724–727 (2015).
- [26] L. X. Yang, Z. K. Liu, Y. Sun, H. Peng, H. F. Yang, T. Zhang, B. Zhou, Y. Zhang, Y. F. Guo, M. Rahn, D. Prabhakaran, Z. Hussain, S. K. Mo, C. Felser, B. Yan, and Y. L. Chen, "Weyl semimetal phase in the noncentrosymmetric compound taas," Nat. Phys. 11, 728– 732 (2015).
- [27] S-Y Xu, C. Liu, S. K. Kushwaha, T.-R. Chang, J. W. Krizan, R. Sankar, C. M. Polley, J. Adell, T. Balasubramanian, K. Miyamoto, N. Alidoust, G. Bian, M. Neupane, I. Belopolski, H.-T. Jeng, C.-Y. Huang, W.-F. Tsai, H. Lin, F. C. Chou, T. Okuda, A. Bansil, R. J. Cava, and M. Z. Hasan, arXiv:1312.7624.
- [28] Z. K. Liu, B. Zhou, Y. Zhang, Z. J. Wang, H. M. Weng, D. Prabhakaran, S.-K. Mo, Z. X. Shen, Z. Fang, X. Dai, Z. Hussain, and Y. L. Chen, "Discovery of a threedimensional topological dirac semimetal, na3bi," Science 343, 864–867 (2014).
- [29] Satya K. Kushwaha, Jason W. Krizan, Benjamin E. Feldman, Andrs Gyenis, Mallika T. Randeria, Jun Xiong, Su-Yang Xu, Nasser Alidoust, Ilya Belopolski, Tian Liang, M. Zahid Hasan, N. P. Ong, A. Yazdani, and R. J. Cava, "Bulk crystal growth and electronic characterization of the 3D Dirac semimetal Na<sub>3</sub>Bi," APL Mat. 3, 041504 (2015).
- [30] Su-Yang Xu, Chang Liu, Satya K. Kushwaha, Raman Sankar, Jason W. Krizan, Ilya Belopolski, Madhab Neupane, Guang Bian, Nasser Alidoust, Tay-Rong Chang, Horng-Tay Jeng, Cheng-Yi Huang, Wei-Feng Tsai, Hsin Lin, Pavel P. Shibayev, Fang-Cheng Chou, Robert J. Cava, and M. Zahid Hasan, "Observation of fermi arc surface states in a topological metal," Science 347, 294–298 (2015).
- [31] Madhab Neupane, Su-Yang Xu, Raman Sankar, Nasser Alidoust, Guang Bian, Chang Liu, Ilya Belopolski, Tay-Rong Chang, Horng-Tay Jeng, Hsin Lin, Arun Bansil, Fangcheng Chou, and M. Zahid Hasan, "Observation of a three-dimensional topological Dirac semimetal phase in high-mobility Cd<sub>3</sub>As<sub>2</sub>," Nat. Commun. 5 (2014).

- [32] Sergey Borisenko, Quinn Gibson, Danil Evtushinsky, Volodymyr Zabolotnyy, Bernd Büchner, and Robert J. Cava, "Experimental Realization of a Three-Dimensional Dirac Semimetal," Phys. Rev. Lett. 113, 027603 (2014).
- [33] Hemian Yi, Zhijun Wang, Chaoyu Chen, Youguo Shi, Ya Feng, Aiji Liang, Zhuojin Xie, Shaolong He, Junfeng He, Yingying Peng, Xu Liu, Yan Liu, Lin Zhao, Guodong Liu, Xiaoli Dong, Jun Zhang, M. Nakatake, M. Arita, K. Shimada, H. Namatame, M. Taniguchi, Zuyan Xu, Chuangtian Chen, Xi Dai, Zhong Fang, and X. J. Zhou, "Evidence of Topological Surface State in Three-Dimensional Dirac Semimetal Cd<sub>3</sub>As<sub>2</sub>," Sci. Rep. 4 (2014).
- [34] Z. K. Liu, J. Jiang, B. Zhou, Z. J. Wang, Y. Zhang, H. M. Weng, D. Prabhakaran, S-K. Mo, H. Peng, P. Dudin, T. Kim, M. Hoesch, Z. Fang, X. Dai, Z. X. Shen, D. L. Feng, Z. Hussain, and Y. L. Chen, "A stable three-dimensional topological Dirac semimetal Cd<sub>3</sub>As<sub>2</sub>," Nat. Mater. 13, 677–681 (2014).
- [35] Tian Liang, Quinn Gibson, Mazhar N. Ali, Minhao Liu, R. J. Cava, and N. P. Ong, "Ultrahigh mobility and giant magnetoresistance in the Dirac semimetal Cd3As2," Nat. Mater. 14, 280–284 (2015).
- [36] L. P. He, X. C. Hong, J. K. Dong, J. Pan, Z. Zhang, J. Zhang, and S. Y. Li, "Quantum Transport Evidence for the Three-Dimensional Dirac Semimetal Phase in Cd<sub>3</sub>As<sub>2</sub>," Phys. Rev. Lett. 113, 246402 (2014).
- [37] Junya Feng, Yuan Pang, Desheng Wu, Zhijun Wang, Hongming Weng, Jianqi Li, Xi Dai, Zhong Fang, Youguo Shi, and Li Lu, "Large linear magnetoresistance in dirac semimetal cd<sub>3</sub>as<sub>2</sub> with fermi surfaces close to the dirac points," Phys. Rev. B 92, 081306 (2015).
- [38] Qiang Li, Dmitri E. Kharzeev, Cheng Zhang, Yuan Huang, I. Pletikosic, A. V. Fedorov, R. D. Zhong, J. A. Schneeloch, G. D. Gu, and T. Valla, arXiv:1412.6543.
- [39] G. E. Volovik, The Universe in a Helium Droplet (Clarendon Press, 2003).
- [40] A A Burkov and Leon Balents, "Weyl Semimetal in a Topological Insulator Multilayer," Phys. Rev. Lett. 107, 127205 (2011).
- [41] A A Zyuzin, Si Wu, and A A Burkov, "Weyl semimetal with broken time reversal and inversion symmetries," Phys. Rev. B 85, 165110 (2012).
- [42] Vivek Aji, "Adler-Bell-Jackiw anomaly in Weyl semimetals: Application to pyrochlore iridates," Phys. Rev. B 85, 241101 (2012).
- [43] Adolfo G Grushin, "Consequences of a condensed matter realization of Lorentz-violating QED in Weyl semimetals," Phys. Rev. D 86, 045001 (2012).
- [44] Chao-Xing Liu, Peng Ye, and Xiao-Liang Qi, "Chiral gauge field and axial anomaly in a Weyl semimetal," Phys. Rev. B 87, 235306 (2013).
- [45] Pallab Goswami and Sumanta Tewari, "Axionic field theory of (3+1)-dimensional Weyl semimetals," Phys. Rev. B 88, 245107 (2013).
- [46] Karl Landsteiner, "Anomalous transport of Weyl fermions in Weyl semimetals," Phys. Rev. B 89, 075124 (2014).
- [47] J. Klier, I. V. Gornyi, and A. D. Mirlin, "Transversal magnetoresistance in weyl semimetals," Phys. Rev. B 92, 205113 (2015).
- [48] Daniel Bulmash and Xiao-Liang Qi, "Quantum oscillations in weyl and dirac semimetal ultrathin films," Phys. Rev. B 93, 081103 (2016).

- [49] Y. Ominato and M. Koshino, "Magnetotransport in the Weyl semimetal in the quantum limit - the role of the topological surface states," ArXiv e-prints (2015), arXiv:1512.08223 [cond-mat.mes-hall].
- [50] Mahito Kohmoto, Bertrand I. Halperin, and Yong-Shi Wu, "Diophantine equation for the three-dimensional quantum hall effect," Phys. Rev. B 45, 13488–13493 (1992).
- [51] Yasumasa Hasegawa, "Energy spectrum of electrons on three dimensional lattice in external magnetic field," Journal of the Physical Society of Japan 61, 1657–1662 (1992), http://dx.doi.org/10.1143/JPSJ.61.1657.
- [52] M. Koshino, H. Aoki, K. Kuroki, S. Kagoshima, and T. Osada, "Hofstadter butterfly and integer quantum hall effect in three dimensions," Phys. Rev. Lett. 86, 1062– 1065 (2001).
- [53] M. Koshino, H. Aoki, T. Osada, K. Kuroki, and S. Kagoshima, "Phase diagram for the hofstadter butterfly and integer quantum hall effect in three dimensions," Phys. Rev. B 65, 045310 (2002).
- [54] Jun Goryo and Mahito Kohmoto, "Polarization of bloch electrons and berry phase in the presence of electromagnetic fields," Phys. Rev. B 66, 085118 (2002).
- [55] M. Koshino and H. Aoki, "Integer quantum hall effect in isotropic three-dimensional crystals," Phys. Rev. B 67, 195336 (2003).
- [56] Mikito Koshino and Hideo Aoki, "Integer quantum hall effect and hofstadter's butterfly spectra in threedimensional metals in external periodic modulations," Phys. Rev. B 69, 081303 (2004).
- [57] J. Brüning, V. V. Demidov, and V. A. Geyler, "Hofstadter-type spectral diagrams for the bloch electron in three dimensions," Phys. Rev. B 69, 033202 (2004).
- [58] Tena Dubček, Colin J. Kennedy, Ling Lu, Wolfgang Ketterle, Marin Soljačić, and Hrvoje Buljan, "Weyl points in three-dimensional optical lattices: Synthetic magnetic monopoles in momentum space," Phys. Rev. Lett. 114, 225301 (2015).
- [59] Miguel A N Araújo and Eduardo V Castro, "Chern band insulators in a magnetic field," Journal of Physics: Condensed Matter 26, 075501 (2014).
- [60] By inspection of the spectrum it seems likely that given a commensurate value of  $\Phi/\Phi_0 = p/q$  there is a particular value of  $k_z$  where q Weyl nodes appear somewhere in the spectrum (not necessarily at E=0). Unfortunately we have no rigorous proof and thus leave it as a conjecture.
- [61] More generally, the degeneracy will be some multiple nq of q for integer, since we know that if n Weyl pairs exist, then we can create nq copies by shifting  $k_y$ . For all the cases considered in this paper, n=1.
- [62] Alexandre Dauphin and Nathan Goldman, "Extracting the chern number from the dynamics of a fermi gas: Implementing a quantum hall bar for cold atoms," Phys. Rev. Lett. 111, 135302 (2013).
- [63] Z. Li, H.-Q. Wang, D.-W. Zhang, S.-L. Zhu, and D.-Y. Xing, "Dynamics of Weyl quasiparticles emerged in an optical lattice," ArXiv e-prints (2016), arXiv:1605.07280 [cond-mat.quant-gas].
- [64] M. Aidelsburger, M. Lohse, C. Schweizer, M. Atala, J. T. Barreiro, S. Nascimbene, N. R. Cooper, I. Bloch, and N. Goldman, "Measuring the Chern number of Hofstadter bands with ultracold bosonic atoms," Nat. Phys. 11, 162–166 (2015).

- [65] Gregor Jotzu, Michael Messer, Remi Desbuquois, Martin Lebrat, Thomas Uehlinger, Daniel Greif, and Tilman Esslinger, "Experimental realization of the topological haldane model with ultracold fermions," Nature 515, 237–240 (2014).
- [66] Markus Greiner, Olaf Mandel, Tilman Esslinger, Theodor W Hänsch, and Immanuel Bloch, "Quantum phase transition from a superfluid to a mott insulator in a gas of ultracold atoms," Nature 415, 39–44 (2002).
- [67] Maxime Ben Dahan, Ekkehard Peik, Jakob Reichel, Yvan Castin, and Christophe Salomon, "Bloch oscillations of atoms in an optical potential," Phys. Rev. Lett. 76, 4508– 4511 (1996).
- [68] Philipp T Ernst, Sören Götze, Jasper S Krauser, Karsten Pyka, Dirk-Sören Lühmann, Daniela Pfannkuche, and Klaus Sengstock, "Probing superfluids in optical lattices by momentum-resolved bragg spectroscopy," Nature Physics 6, 56–61 (2010).
- [69] A uniform population of the band is expected if the hierarchy of energy scales  $\Delta \gg k_B T \gg W$  is satisfied, where W is the bandwidth  $\Delta$  is the band gap and  $k_B T$  is the temperature energy scale. This criterion is satisfied for high flatness ratios, which have been demonstrated in experiment [64].
- [70] Di Xiao, Ming-Che Chang, and Qian Niu, "Berry phase effects on electronic properties," Rev. Mod. Phys. 82, 1959–2007 (2010).
- [71] P Streda, "Theory of quantised hall conductivity in two dimensions," Journal of Physics C: Solid State Physics 15, L717 (1982).
- [72] Immanuel Bloch, Jean Dalibard, and Wilhelm Zwerger, "Many-body physics with ultracold gases," Rev. Mod. Phys. 80, 885–964 (2008).
- [73] Y.-Q. Wang and X.-J. Liu, "A Scaling Behavior of Bloch Oscillation in Weyl Semimetals," ArXiv e-prints (2016), arXiv:1605.02671 [cond-mat.mes-hall].
- [74] Xiong-Jun Liu, K. T. Law, and T. K. Ng, "Realization of 2d spin-orbit interaction and exotic topological orders in cold atoms," Phys. Rev. Lett. 112, 086401 (2014).
- [75] Pallab Goswami and Sudip Chakravarty, "Quantum criticality between topological and band insulators in 3 + 1 dimensions," Phys. Rev. Lett. 107, 196803 (2011).
- [76] Hiroki Isobe and Naoto Nagaosa, "Theory of a quantum critical phenomenon in a topological insulator: (3+1)dimensional quantum electrodynamics in solids," Phys. Rev. B 86, 165127 (2012).
- [77] Gregory Gorohovsky, Rodrigo G. Pereira, and Eran Sela, "Chiral spin liquids in arrays of spin chains," Phys. Rev. B 91, 245139 (2015).
- [78] Chui-Zhen Chen, Juntao Song, Hua Jiang, Qing-feng Sun, Ziqiang Wang, and X. C. Xie, "Disorder and metalinsulator transitions in weyl semimetals," Phys. Rev. Lett. 115, 246603 (2015).
- [79] M. H. Anderson, J. R. Ensher, M. R. Matthews, C. E. Wieman, and E. A. Cornell, "Observation of boseeinstein condensation in a dilute atomic vapor," Science 269, 198–201 (1995).
- [80] K. B. Davis, M. O. Mewes, M. R. Andrews, N. J. van Druten, D. S. Durfee, D. M. Kurn, and W. Ketterle, "Bose-einstein condensation in a gas of sodium atoms," Phys. Rev. Lett. 75, 3969–3973 (1995).
- [81] C. C. Bradley, C. A. Sackett, J. J. Tollett, and R. G. Hulet, "Evidence of bose-einstein condensation in an atomic gas with attractive interactions," Phys. Rev. Lett.

**75**, 1687–1690 (1995).

- [82] Markus Greiner, Cindy A. Regal, and Deborah S. Jin, "Emergence of a molecular bose-einstein condensate from a fermi gas," Nature 426, 537 (2003).
- [83] C. A. Regal, M. Greiner, and D. S. Jin, "Observation of resonance condensation of fermionic atom pairs," Phys. Rev. Lett. 92, 040403 (2004).
- [84] S. Jochim, M. Bartenstein, A. Altmeyer, G. Hendl, S. Riedl, C. Chin, J. Hecker Denschlag, and R. Grimm, "Bose-einstein condensation of molecules," Science 302, 2101 (2003).
- [85] M. W. Zwierlein, C. A. Stan, C. H. Schunck, S. M. F. Raupach, S. Gupta, Z. Hadzibabic, and W. Ketterle, "Observation of bose-einstein condensation of molecules," Phys. Rev. Lett. 91, 250401 (2003).
- [86] Colin J. Kennedy, William Cody Burton, Woo Chang Chung, and Wolfgang Ketterle, "Observation of boseeinstein condensation in a strong synthetic magnetic field," Nat Phys 11, 859 (2015).
- [87] X.G. Wen and A. Zee, "Winding number, family index theorem, and electron hopping in a magnetic field," Nuclear Physics B **316**, 641 662 (1989).
- [88] F. D. M. Haldane, "Model for a quantum hall effect without landau levels: Condensed-matter realization of the "parity anomaly"," Phys. Rev. Lett. 61, 2015–2018 (1988).

## Using the spread of a wavepacket to probe the distance between Weyl nodes.

In this section, we illustrate how tuning the spread of wavepackets without changing the average momentum can be used to reconstruct the Chern number profile. In particular, by tuning parameters such as temperature, density, trapping profile, and lattice depth [66, 72, 79–85], cold atom experiments routinely realize a wide variety of momentum-space distributions. Furthermore, the distribution can not only be tuned via experimentally-accessible parameters, but measured with high accuracy in time-of-flight. As discussed in the main text, this tunability of the momentum profile in the z-direction can be directly used to measure the Chern number profile as a function of  $k_z$ . In this appendix, we will show a particular example of such a fitting procedure.

To model a wavepacket with finite momentum spread, we pick the simplest case of a Gaussian profile centered around  $k_z=0$  with width  $\sigma$ 

$$W(k_z) = \frac{1}{\sqrt{2\pi}\sigma} \frac{e^{-k_z^2/2\sigma^2}}{\text{Erf}(\pi/\sqrt{2}\sigma)},$$
 (8)

where the error function (Erf) results from normalizing the Gaussian distribution over the compact Brillouin zone. The Hall drift in the (x,y) plane would then yield an non-quantized effective Chern number given by the actual Chern number profile  $\mathcal{C}_{k_z}$  averaged over the Brillouin zone and weighted by  $W(k_z)$ :

$$C_{\text{eff}} = \sum_{k_z = -\pi}^{\pi} W(k_z) C_{k_z}. \tag{9}$$

Consider the case as in our model of the Weyl semimetal where (possibly degenerate) Weyl nodes occur at  $k_z = \pm K_0/2$ . The Chern number profile follows  $\mathcal{C}_{k_z} = \mathcal{C}_{k_z=0}$  for  $|k_z| < K_0/2$ , and  $\mathcal{C}_{k_z} = \mathcal{C}_{k_z=\pi}$  otherwise (cf. Fig. 2 of the main text). Hence, the problem has now been reduced to inferring three quantities, namely  $K_0$ ,  $\mathcal{C}_{k_z=0}$  and  $\mathcal{C}_{k_z=\pi}$ , from measurements of  $\mathcal{C}_{\text{eff}}$  for various values of  $\sigma$ .

Taking a wavepacket that is well-localized near  $k_z=0$  such as a Bose-Einstein condensate [79–81] corresponds to  $\sigma \approx 0$ . Inspection of Eqs. (8) and (9), trivially reveals that  $\mathcal{C}_{\text{eff}}(\sigma=0)=\mathcal{C}_{k_z=0}$ . Hence, the Hall drift with a wavepacket localized in  $k_z$  would yield  $\mathcal{C}_{k_z=0}$ , one of the three quantities of interest.

The other extreme limit, a "high-temperature" wavepacket completely delocalized in  $k_z$  (while remaining in the lowest band) has uniform distribution  $W(k_z) = 1/2\pi$ . In this limit,  $\mathcal{C}_{\text{eff}}$  would saturate to

$$C_{\text{sat}} = C_{k_z = \pi} - (C_{k_z = \pi} - C_{k_z = 0}) K_0 / 2\pi,$$
 (10)

as mentioned in the main text.  $C_{\text{sat}}$  relates the remaining two quantities of interest,  $K_0$  and  $C_{k_z=\pi}$ .

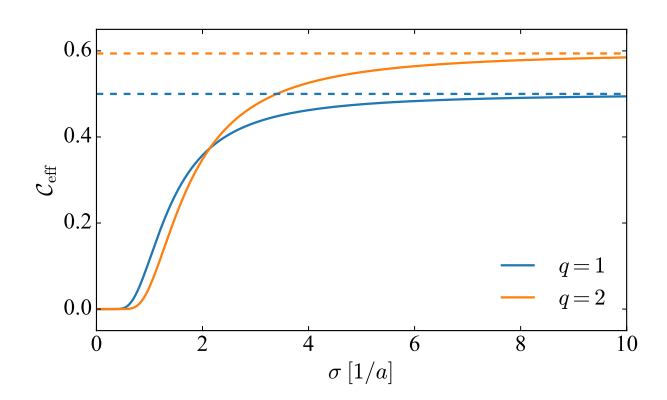


FIG. 5.  $\mathcal{C}_{\text{eff}}$  as a function of  $\sigma$  for the two cases corresponding to Fig. 2 of the main text. The dashed lines correspond to the  $\mathcal{C}_{\text{sat}}$  values calculated from Eq. (10).

The behavior of  $C_{\text{eff}}$  as a function of the width of the wavepacket in between these two limits is shown in Fig. 5. For small  $\sigma$  there is flat plateau at  $C_{k_z=0}$  as the wavepacket has all its weight in the  $C_{k_z} = C_{k_z=0}$  region of the Brillouin zone for  $\sigma \ll K_0$ . Beyond this threshold, the tails of Gaussian (8) pick up contributions from the  $C_{k_z} = C_{k_z=\pi}$  region and  $C_{\text{eff}}$  deviates from the plateau. Therefore, the length of this plateau is directly related to the separation of the Weyl nodes,  $K_0$ . To determine this quantity it is useful to define empirically

$$|\mathcal{C}_{\text{eff}}(\sigma_{\Lambda}) - \mathcal{C}_{k_z=0}| = \Lambda,$$
 (11)

where  $\Lambda \ll |\mathcal{C}_{k_z=0} - \mathcal{C}_{k_z=\pi}|$ , and  $\sigma_{\Lambda}$  is the empirical length of the plateau. Using the asymptotic properties of the error function, Eq. (11) can be reduced to

$$\frac{2\sqrt{2}\sigma_{\Lambda}}{K_{0}}e^{-K_{0}^{2}/8\sigma_{\Lambda}^{2}} = \Lambda |\mathcal{C}_{k_{z}=\pi} - \mathcal{C}_{k_{z}=0}|, \qquad (12)$$

which can further simplified using Eq. (10) to

$$\frac{2\sqrt{2}\sigma_{\Lambda}}{K_0} \left( 1 - \frac{K_0}{2\pi} \right) e^{-K_0^2/8\sigma_{\Lambda}^2} = \Lambda |\mathcal{C}_{\text{sat}} - \mathcal{C}_{k_z=0}|. \quad (13)$$

Note that  $C_{\text{sat}}$  and  $C_{k_z=0}$  are experimentally accessible quantities and  $\sigma_{\Lambda}$  is an empirically chosen quantity. Hence, solving the transcendental equation (13) the value of  $K_0$  can be obtained and used in Eq. (10) to obtain  $C_{k_z=\pi}$ . One may also perform a simple three parameter fit given the measured profile  $W(k_z)$  and obtain these parameters without any further analytical insight.

We have therefore shown that from experimentally-realistic procedures it is indeed possible to reconstruct the Chern number profile of a Weyl semimetal. We note that in the absence of interactions these topological properties of the band structure are in principle equally accessible via boson or fermions. Indeed, condensation has recently been measured in a two-dimensional Hofstadter model that can be thought of as a precursor to the Weyl semimetal [86]. Combined with wave packet measurements of Hall drift and Chern number that have been demonstrated in similar two-dimensional models [64, 65], these ideas for probing the topological physics of the Weyl semimetal should be well within the reach of current technology.

## Weyl nodes at rational fluxes

The fractal nature of the Weyl butterfly suggests that Weyl nodes may appear not just at some values of rational flux  $\Phi = \Phi_0 p/q$ , but for all rational fluxes. Our numerics confirm the emergence of q pairs of Weyl nodes at all rational fluxes that we have checked. In this section we provide a plausibility argument for this claim, though an analytic proof currently eludes us.

We start by noting that the effective 2D Hamiltonian obtained by considering the Weyl semimetal Hamiltonian (Eq. (1) in the main text) at a fixed  $k_z$  slice can be decomposed into three kinds of terms, the intra-sublattice hoppings  $(J_1)$ , the inter-sublattice hoppings  $(J_2)$ , and a staggered chemical potential  $M_{\rm eff} = M - J_1 \cos k_z$ . For  $J_2$ =0, the Hamiltonian represents two decoupled square lattices; the spectra of each of these copies are shifted in energy by  $\pm M_{\rm eff}$ .

It was shown by Wen and Zee [87] that the singleparticle spectrum of fermions hopping on a square lattice with a magnetic flux  $\Phi$  per plaquette has at least q isolated nodes at zero energy for q even. This implies that the spectrum of Hamiltonian Eq. (1) at a fixed  $k_z$  and  $J_2 = 0$  has 2q nodes (q nodes per sublattice) with q located at  $E = M_{\text{eff}}$  and q at  $E = -M_{\text{eff}}$ . However, a  $J_2 \neq 0$  induces a mixing between the spectra of the two sublattices making the q pairs of nodes gapped. Such inter-sublattice hopping is analogous to a Haldanelike topological gap [88] effectively breaking time-reversal symmetry. As long as the two competing gaps, due to  $M_{\text{eff}}$  and  $J_2$ , are of the same order, the spectrum can be fine-tuned by varying  $k_z$  to find gapless nodes in the spectrum. The periodicity of the Brillouin zone ensures that there are q of them and since the spectrum depends on  $k_z$  via  $\cos(k_z)$ , the spectra at  $\pm k_z$  are identical thus resulting in q-pairs of nodes.